rechargeable lithium-ion batteries after prolonged cycling, Electrochim. Acta 47 1899-1911.

13. N. Philip, P. Stefano, W. Martin (2013), *Interface Investigations of a Commercial Lithium Ion Battery Graphite Anode Material by Sputter Depth Profile X-ray Photoelectron Spectroscopy*, *Langmui*r 29 5806-5816.

14. Wang, S. Kadam, H. Li, S. Shi, Y. Qi (2018), *Review on modeling of the anode solid electrolyte interphase (SEI) for lithium-ion batteries*, Npj Comput. Mater. 4 1-26.

KHẢO SÁT CÁC ĐẶC TRƯNG ĐIỆN HÓA CỦA PIN LITI-ION THƯƠNG MẠI DẠNG TRỤ

Tóm tắt: *Pin liti-ion thương mại dạng trụ, kiểu dáng 26650, có dung lượng danh định 4000 mAh đã được tháo dỡ phục vụ nghiên cứu cấu trúc và thành phần cấu tạo của vật liệu điện cực. Các phép phân tích nhiễu xạ tia X (X-ray), hiển vi điện tử quét (SEM), phổ tán xạ năng lượng tia X (EDX) cho thấy vật liệu dương cực là hỗn hợp của các ôxít $LiMn_2O_4$ và $LiMO_2$ (M = Mn, Co, Ni), vật liệu âm cực là graphit. Vật liệu dương cực được cấu tạo từ các hạt ôxít tương đối đồng đều với đường kính trung bình trong khoảng từ 1-3 µm, vật liệu âm cực là các hạt graphit với đường kính trung bình khoảng 10 µm. Dung lượng xả của pin ở chu kỳ đầu tiên là 3820 mAh (tương ứng khoảng 95,5% dung lượng danh định). Dung lượng pin giảm dần trong các chu kì phóng, nạp tiếp theo. Hiệu điện thế hoạt động trung bình của quá trình phóng là 3.7 V, giá trị này tương đồng với hiệu điện thế hoạt động danh định của pin.*

Từ khóa*: Pin liti-ion, pin thương mại, vật liệu âm cực, vật liệu dương cực, hợp chất liti.*

FLAPW METHOD AND PRACTICAL CALCULATION FOR Gd CRYSTAL: ELECTRONIC STRUCTURE AND MAGNETIC PHASE STABILITY

Tran Van Quang

University of Transport and Communications

Abstact: *Description and understanding of electronic structures and magnetic properties of gadolinium Gd have been challenging. Especially, its magnetic phase stability of gadolinium has been in debate for a long time. In this report, the precise all-electron full-potential linearized augmented plane wave (FLAPW) method is introduced to study properties of Gd. Due to strongly localized f-states, the calculation may lead to weird results depending on defined parameters. The calculations including both 4f-core and 4f-band models are performed. The analysis of the electronic structure and magnetic phase stability are shown and discussed. All the results are good agreement with available experiments and previous theoretical reports.*

Keywords: *Gd phase stability, band structure, f-core model, f-band model, FLAPW method.*

Received: 15 March 2020

Accepted for publication: 20 April 2020

Email: tranquang@utc.edu.vn

1. INTRODUCTION

In modern material science, the economy-efficient approach to explore is using the density functional theory [1] proposed by Honhenberg, Kohn and Sham. The core of the theory is Kohn – Sham equation (in atomic unit) [2],

$$\left\{-\frac{\Delta}{2} + v(\vec{r}) + \int \frac{\rho(\vec{r}\prime)}{|\vec{r}-\vec{r}\prime|} d\vec{r}' + v_{xc}[\rho(\vec{r})]\right\}\psi_i = \varepsilon_i\psi_i, \quad (1)$$

$$\rho(\vec{r}) = \sum_{i=1}^{N} n_i \langle\psi_i|\psi_i\rangle, \quad (2)$$

is electron density, n the occupation number, $v_{xc}[\rho]=\delta E_{xc}[\rho]/\delta\rho$ the exchange-corelation potential, and v the external potential. One can solve this equation self-consistenly [3]. The

seft-consistently converged solution obtained gives us information of the ground states, e.g. eigenvalues ε_i, total energy, forces, and etc. [3] Nevertheless, this task is very demanding and the method to solve is still being developed in different ways, e.g. to deal with exchange correlation potential [4–6] and to develop numerical methods. Practically, when working on a magnetic system, many local minima may occur basically which infer multi-solutions. Some of the solutions are therefore unphysical meaning. Especially, in the case of strongly localized system such as Gd bulk (the well-known rare earth materials), the calculations may contain gosh states which originate from the strongly localized f states. As in general, the electron-nuclear interaction is given by the bare Cloulomb interaction whereas exchange correlation is very tough to describe. The strongly localized f states affect drastically in both of them. There are two classes of electrons: valence electrons (participate actively in chemical bonding), and core electrons (tightly bound to the nuclei, do not participate in bonding and to be treated as frozen orbitals). There is a third class of electrons called semi-core electrons. The f electrons usually are in this class. Its wave functions polarizes. There are two way to treat the problam: pseudopotential methods and all-electron methods. The precise all-electron full-potential linearized augmented plane wave (FLAPW) method is one of the most precise all electron method [3–5]. In this report we will present some matrix elements within FLAPW method. The exchange correlation potential will be treated by using local density approximation (LDA) [7]. The numerical results will be shown and discussed.

2. CONTENT

2.1. Hamiltonian matrix in FLAPW method

To solve Kohn-Sham equation, orbitals ψ are written as a linear combination of a complete basis set, i.e.

$$\psi_i(\vec{r}) = \sum_{\alpha}^{M} c_{i\alpha}\varphi_\alpha(\vec{r}). \quad \text{(M is dimension of the basis orbitals)} \tag{3}$$

For the specific basis set ϕ, in FLAPW, it is chosen by deviding space into interstitial and muffin-tin regions (here we are interested in 3D bulk calculations, if 2D oe 1D needed vacuum should be included) [3]

$$\varphi_{E_l}^{(\vec{k})} = \begin{cases} \dfrac{1}{\sqrt{\Omega}}\sum_{\vec{G}} c_{\vec{G}} e^{i(\vec{k}+\vec{G})\vec{r}} \ \text{ in the interstitial region}: \ |\vec{r}-\vec{R}| > r_{mt} \\ \sum_{l,m}\left[a_{lm}^{\mu,(\vec{k})}(E_l)u_l^\mu(r) + b_{lm}^{\mu,(\vec{k})}(E_l)\dot{u}_l^\mu(r)\right] Y_{lm}(\vec{r}^\mu) \\ \text{in the } a\text{tomic region muffin-tin } \mu: \ |\vec{r}-\vec{R}| < r_{mt} \end{cases} \tag{4}$$

In the muffin-tin region, these two radial wave functions are (i) the solutions of the radial Schrödinger equation, u_l, solved at a fixed energy, E_l; (atom unit)

$$\left(-\frac{d^2}{dr^2}+\frac{l(l+1)}{r^2}u_l(r)+V(r)-E_1\right)ru_l(r)=0, \tag{5}$$

and (ii) their derivatives $\dot{u}_l$. Y_{lm} are spherical harmonics and the coefficients a_{lm} and b_{lm} are determined by the requirement that the plane waves and their radial derivatives are continuous at the muffin-tin boundary. For the potential, there is no shape approximation assumed [3,8]

$$V(\vec{r})=\begin{cases}\sum_{\vec{G}} V_I^{\vec{G}} e^{i\vec{G}\vec{r}} & \text{interstitial}\\ \sum_{lm} V_{MT}^{lm}(r)Y_{lm}(\vec{r}_\mu) & \text{muffin-tin}\end{cases}, \tag{6}$$

Accordingly, hamiltonian and overlap matrices consist of two contributions from the two regions where space is divided, i.e. $H=H_I+H_{MT}$ and $S=S_I+S_{MT}$ in which *I* stands for "Interstitial" and *MT* "muffin-tin"

Contribution of muffin-tins. Let denote the quantum states as follow: $lm \to L;\ \ u_l Y_{lm} \to \varphi_L$. The contribution of muffin-tin to the Hamiltonian and overlap matrices are is given by inserting Eqs. (3,4) into Eqs. (2) and (1) to obtain

$$\begin{aligned}H_{MT}^{\vec{G}\prime\vec{G}}(\vec{k}) = \sum_\mu \int_{MT^\mu} d\vec{r} \sum_{L\prime}\Big(a_{L\prime}^{\mu\vec{G}}(\vec{k})\varphi_{L\prime}^{\alpha}(\vec{r}) + \\ +b_{L\prime}^{\mu\vec{G}}(\vec{k})\dot{\varphi}_{L\prime}^{\alpha}(\vec{r})\Big)^* H_{MT^\alpha}\sum_L\Big(a_L^{\mu\vec{G}}(\vec{k})\varphi_L^{\alpha}(\vec{r})+b_L^{\mu\vec{G}}(\vec{k})\dot{\varphi}_L^{\alpha}(\vec{r})\Big),\end{aligned} \tag{7}$$

$$\begin{aligned}S_{MT}^{\vec{G}\prime\vec{G}}(\vec{k}) = \sum_\mu \int_{MT^\mu} d\vec{r} \sum_{L\prime}\Big(a_{L\prime}^{\mu\vec{G}}(\vec{k})\varphi_{L\prime}^{\alpha}(\vec{r}) + \\ +b_{L\prime}^{\mu\vec{G}}(\vec{k})\dot{\varphi}_{L\prime}^{\alpha}(\vec{r})\Big)^* \sum_L\Big(a_L^{\mu\vec{G}}(\vec{k})\varphi_L^{\alpha}(\vec{r})+b_L^{\mu\vec{G}}(\vec{k})\dot{\varphi}_L^{\alpha}(\vec{r})\Big),\end{aligned} \tag{8}$$

These contain the following type of matrix elements

$$t_{L'L}^{\alpha\varphi\varphi}(\vec{k}) = \int_{MT^{\mu}} d\vec{r}\left(\varphi_{L'}^{\alpha}(\vec{r})\right)^{*} H_{MT^{\alpha}} \varphi_{L}^{\alpha}(\vec{r}) \tag{9}$$

H can be splited into two parts, the spherical H_{sp} and the nonspherical contributions V_{ns}, i.e.

$$H_{MT^{\alpha}} = H_{sp}^{\alpha} + V_{ns}^{\alpha} \tag{10}$$

Note that $\phi_{L}^{\alpha}, \dot{\phi}_{L}^{\alpha}$ can be chosen to diagonalize H_{sp}

$$H_{sp}^{\alpha}\varphi_{L}^{\alpha} = E_{l}\ \ \varphi_{L}^{\alpha}, \tag{11}$$

$$H_{sp}^{\alpha}\dot{\varphi}_{L}^{\alpha} = E_{l}\ \ \dot{\varphi}_{L}^{\alpha} + \varphi_{L}^{\alpha}. \tag{12}$$

Taking inner product with $\langle\varphi_{L}^{\alpha}|, \langle\dot{\varphi}_{L}^{\alpha}|$ respectively gives

$$\langle\varphi_{L'}^{\alpha}\left|H_{sp}^{\alpha}\varphi_{L}^{\alpha}\right\rangle_{MT^{\alpha}} = E_{l}\ \ \delta_{ll'}\delta_{mm'}, \qquad \langle\varphi_{L'}^{\alpha}|\varphi_{L}^{\alpha}\rangle_{MT^{\alpha}} = \delta_{ll'}\delta_{mm'}, \tag{13}$$

$$\langle\dot{\varphi}_{L'}^{\alpha}\left|H_{sp}^{\alpha}\varphi_{L}^{\alpha}\right\rangle_{MT^{\alpha}} = 0, \qquad \langle\dot{\varphi}_{L'}^{\alpha}|\varphi_{L}^{\alpha}\rangle_{MT^{\alpha}} = 0, \tag{14}$$

$$\langle\varphi_{L'}^{\alpha}\left|H_{sp}^{\alpha}\dot{\varphi}_{L}^{\alpha}\right\rangle_{MT^{\alpha}} = \delta_{ll'}\delta_{mm'}, \quad \langle\varphi_{L'}^{\alpha}\left|H_{sp}^{\alpha}\dot{\varphi}_{L}^{\alpha}\right\rangle_{MT^{\alpha}} = \langle\varphi_{L'}^{\alpha}\left|E_{l}\ \ \dot{\varphi}_{L}^{\alpha} + \varphi_{L}^{\alpha}\right\rangle_{MT^{\alpha}} = \delta_{ll'}\delta_{mm'}, \tag{15}$$

$$\langle\dot{\varphi}_{L'}^{\alpha}\left|H_{sp}^{\alpha}\dot{\varphi}_{L}^{\alpha}\right\rangle_{MT^{\alpha}} = E_{l}\ \ \delta_{ll'}\delta_{mm'}\langle\dot{u}_{l}^{\alpha}|\dot{u}_{l}^{\alpha}\rangle_{MT^{\alpha}}, \qquad \langle\dot{\varphi}_{L'}^{\alpha}|\dot{\varphi}_{L}^{\alpha}\rangle_{MT^{\alpha}} = \delta_{ll'}\delta_{mm'}\langle\dot{u}_{l}^{\alpha}|\dot{u}_{l}^{\alpha}\rangle_{MT^{\alpha}}. \tag{16}$$

It is noted that the potential is also expanded by using spherical harmonics, i.e.

$$V^{\alpha}(\vec{r}) = \sum_{L''} V_{L''}^{\alpha}(\vec{r}) Y_{L''}(\vec{r}). \tag{17}$$

Thus, hamiltonian matrix is obtained

$$H_{MT}^{\vec{G}'\vec{G}}(\vec{k}) = \\ = \sum_{\mu}\sum_{L'}\left[\begin{array}{c}\left(a_{L'}^{\mu\vec{G}'}(\vec{k})\right)^{*} t_{L'L}^{\alpha\varphi\varphi} a_{L}^{\mu\vec{G}}(\vec{k}) + \left(b_{L'}^{\mu\vec{G}'}(\vec{k})\right)^{*} t_{L'L}^{\alpha\dot{\varphi}\dot{\varphi}} b_{L}^{\mu\vec{G}}(\vec{k}) + \\ + \left(a_{L'}^{\mu\vec{G}'}(\vec{k})\right)^{*} t_{L'L}^{\alpha\varphi\dot{\varphi}} b_{L}^{\mu\vec{G}}(\vec{k}) + \\ + \left(b_{L'}^{\mu\vec{G}'}(\vec{k})\right)^{*} t_{L'L}^{\alpha\dot{\varphi}\varphi} a_{L}^{\mu\vec{G}}(\vec{k})\end{array}\right] \tag{18}$$

Where

$$t_{L'L}^{\alpha\varphi\varphi} = \sum_{l"} I_{l'll"}^{\alpha uu} G_{l'll"}^{m'mm"} + \delta_{ll}\,\delta_{mm'} E_l,$$

$$G_{l'll"}^{m'mm"} = \int Y_{lm}^{*} Y_{l'm'} Y_{l"m"} d\Omega\,, \tag{19}$$

$$I_{l'l"}^{\alpha uu} = \int u_{l'}^{\alpha}(r) u_{l}^{\alpha}(r) V_{l"}^{\alpha}(r) r^2 dr$$

.

Similarly, the overlap matrix is

$$S_{MT}^{\vec{G}'\vec{G}}(\vec{k}) = \sum_{\mu} \sum_{L'} \left[\left(a_{L'}^{\mu\vec{G}'}(\vec{k}) \right)^{*} a_{L}^{\mu\vec{G}}(\vec{k}) + \left(b_{L'}^{\mu\vec{G}'}(\vec{k}) \right)^{*} b_{L}^{\mu\vec{G}}(\vec{k}) \right] \langle \dot{u}_l^{\alpha} | \dot{u}_l^{\alpha} \rangle_{MT^{\alpha}} \tag{20}$$

The interstitial contribution. Using basis function (4) for the interstitial region, the hamiltonian matrix is derived by noting that the kinetic energy is diagonal in momentum space and the potential is local, diagonal in real space and of convolution form in momentum space,

$$H_I^{\vec{G}\vec{G}'}(\vec{k}) = -\frac{\hbar^2}{2m} |\vec{G} + \vec{k}|^2 \delta_{\vec{G}\vec{G}'} + V(\vec{G} - \vec{G}');\;\; S_I^{\vec{G}\vec{G}'} = \delta_{\vec{G}\vec{G}'}, \tag{21}$$

The muffin-tin *a*- and *b*-coefficients are determined by expanding planewave into spherical harmonics using Rayleigh expansion, i.e.

$$e^{i\vec{K}\vec{r}} = 4\pi \sum i^l j_l(rK) Y_L^{*}(\vec{K}) Y_L\;(\vec{r}), \tag{22}$$

where $r = |\vec{r}|;\;\; \vec{K} \equiv \vec{G} + \vec{k};\;\; K = |\vec{K}|$. The requirement of continuity of the wave functions at the muffin-tin boundary leads the coefficients *a* and *b* [9]

$$a_L^{\mu\vec{G}}(\vec{k}) = e^{i\vec{K}\vec{\tau}^{\mu}} \frac{4\pi i^l}{W} Y_L^{*}(\vec{R}^{\mu}\vec{K}) \left[\dot{u}_l(R_{MT^{\alpha}}) K j'_l\;(R_{MT^{\alpha}}K) - \dot{u}'_l(R_{MT^{\alpha}}) K j_l\;(R_{MT^{\alpha}}K) \right], \tag{23}$$

$$b_L^{\mu\vec{G}}(\vec{k}) = e^{i\vec{K}\vec{\tau}^{\mu}} \frac{4\pi i^l}{W} Y_L^{*}(\vec{R}^{\mu}\vec{K}) \left[u'_l(R_{MT^{\alpha}}) K j_l\;(R_{MT^{\alpha}}K) - u_l(R_{MT^{\alpha}}) K j'_l\;(R_{MT^{\alpha}}K) \right], \tag{24}$$

With

$$W = \dot{u}_l(R_{MT^\alpha})u'_l(R_{MT^\alpha}) - u_l(R_{MT^\alpha})\dot{u}'_l(R_{MT^\alpha}). \quad (25)$$

The density therefore can be obtained by tanking inner product from Eq. (2)

2.2. Numerical results

In numberical calculation for Gd pristine crystal, we used hexagonal structure with lattice constants a =6.89 au and c=10.92 au. The star-function cut-off, *Gmax*, is 11.5. The plane-wave cut off *Kmax* is 3.8. The spin polarization has been included. For the k-point mesh, we use 17×17×9 Monkhorst-Pack grids. The initial spin polarization is provided by starting magnetic moments of 7.0μ_B and 7.0μ_B. At first, Gd-4f states are treated as core. In this model so-called 4f-core model, we vary the lattice constants a and c and calculate the corresponding total energies. The results are presented in FIG. 1. This calculation shows the equilibrium lattice constants, i.e. a = 6.79 au and c = 10.80 au.

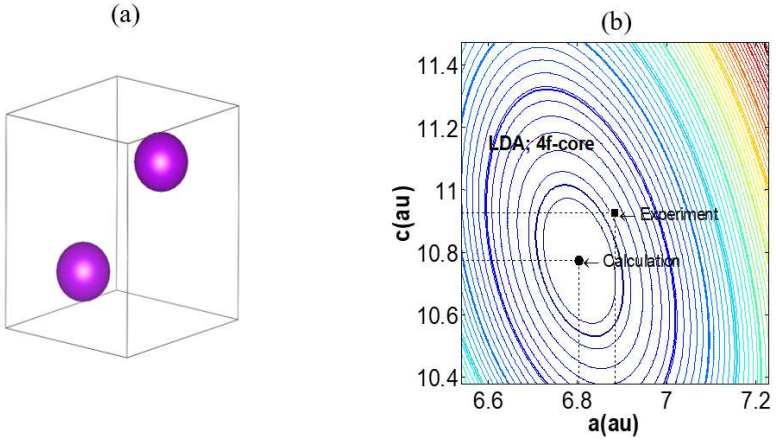

Fig. 1. *(a) Crystal structure of Gd and (b) its energy mesh. The minimum value infers the equilibirum lattice constants.*

Table 1. **Equilibrium lattice constants and total magnetic moments within LDA calculation in 4f-core model together with experimental result.**

	a(au)			$\mu_{tot}(\mu B)$
LDA	6.79	c(au)	c/a	7.81
Experiment	6.88	10.92	1.59	7.63

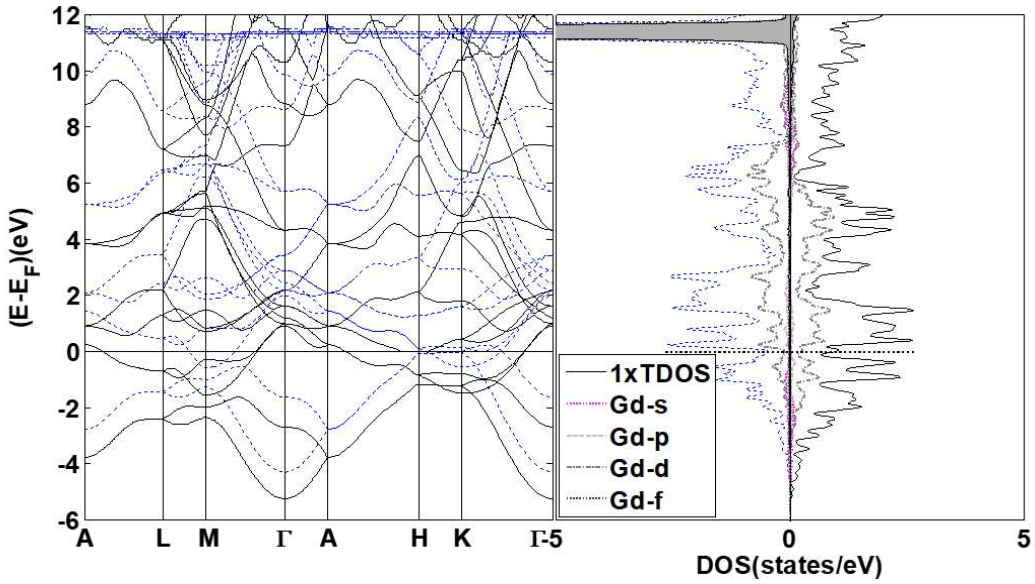

Fig. 2. *Band structure calculation and Density of states within LDA calculation and 4f-core model*

As can be seen, in the 4f-core model, calculation using LDA gives slightly underestimated equiriblium lattice constants as it does [6,10]. The results still are very well consistent with experiments and theoretical reports earlier [11]. The magnetic moment has been reported to be 7.41μ_B whereas our result shows 7.81μ_B and the experiment result is 7.63μ_B. Our calculated result is only 2.4% larger than the experimental value.

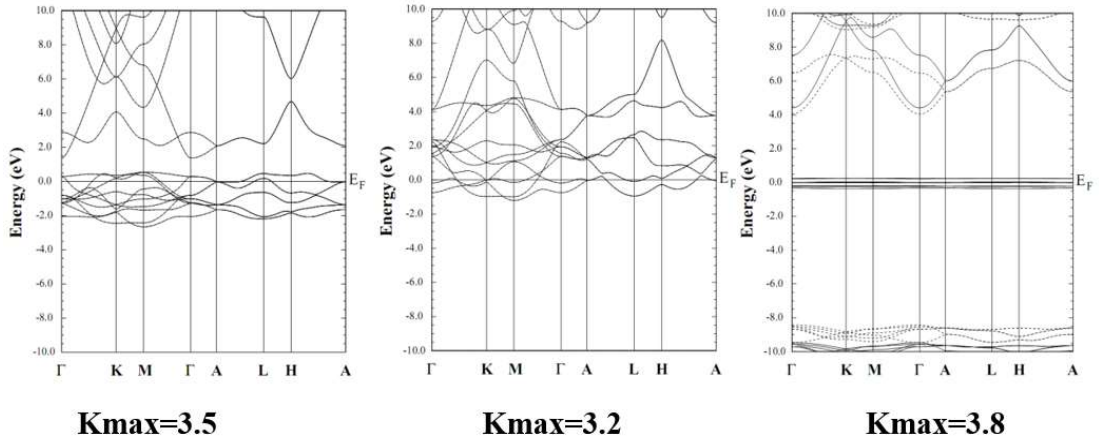

Fig. 3. *Band structure of Gd in 4f-band model with different Kmax values. Ghost states result in weird band structures.*

To continue, we examine the band structure of Gd. The results are presented in FIG. 2. As can be seen, 4f bands are disappeared from the valence band structure. It is well agreed with results reported of Ph Kurz et al. using all-electron FLAPW-FLEUR package [11].

In 4f-band model in which 4f electrons is treated as valence electrons, by using the experimental lattice constants, we found that some gosh states occur. These lead to weird results as shown in FIG. 3. These unrelevant results stem from chosing unappropriate parameters such as *Kmax* values and the gosh states appears during self-consistently solving.

Therefore, the parameters invoked must be opted to be very careful. After a number of tests, here we present the calculations with Gmax= 11.5, Kmax=3.8. We obtained relevant results, as presented in FIG. 4 for LDA calculation

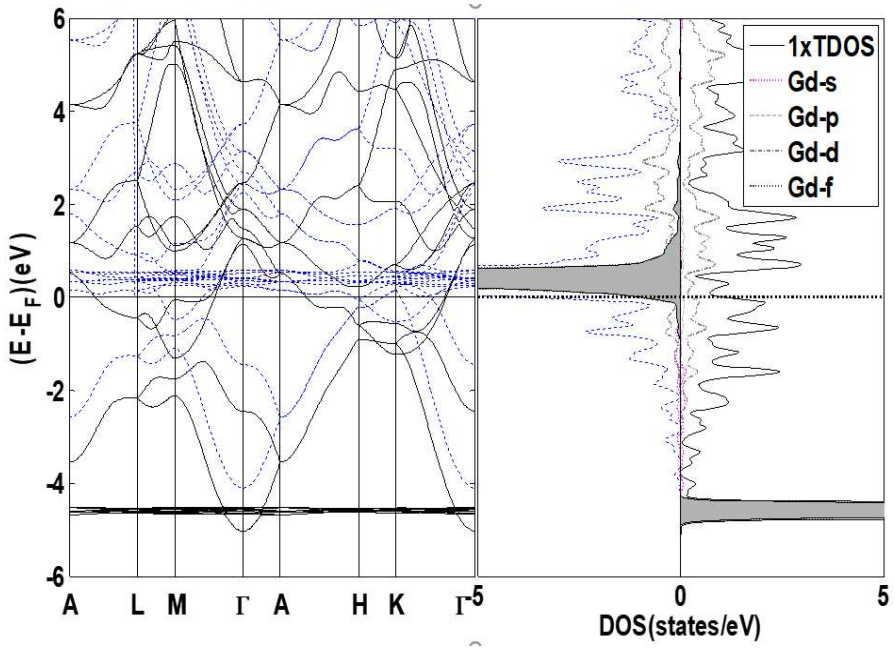

Fig. 4. *Band structure calculation and DOS within LDA calculation and 4f-band model*

As can be seen, within LDA calculation, Gd-4f states localize strongly at around -4.5 eV from the Fermi energy for majority spin and right beside the Fermi energy for the minority spin. The latter alters the band near the Fermi energy thereby the chemical bonding and the phase stability of Gd crystal. To take into account the effect of on-site interactions from f bands, Hubbard U correction is adapted, i.e. LDA+U calculation with the correlation energies of U_d = 5.0eV; J_d = 1.0eV and U_f = 7.7eV; J_d = 0.7eV [11–17]. The calculated electronic band structure is presented in FIG. 5. As shown, the on-site interaction with U and J corrections pushes majority and minority spins away. The majority spin locates at ~ -10.3 eV (deep) below Fermi energy. This explains why 4f-core model works for some cases, e.g. band structure as presented above, and 4f electrons play as semi-core electrons. The minority spin is at ~1.8eV above Fermi energy. The calculated results are excellent agreement with previous publications [11–14,18,19]. Note that all the calculations have been done by assuming that FM phase is stable. Next step, we will demonstrate that FM ordering is indeed stable.

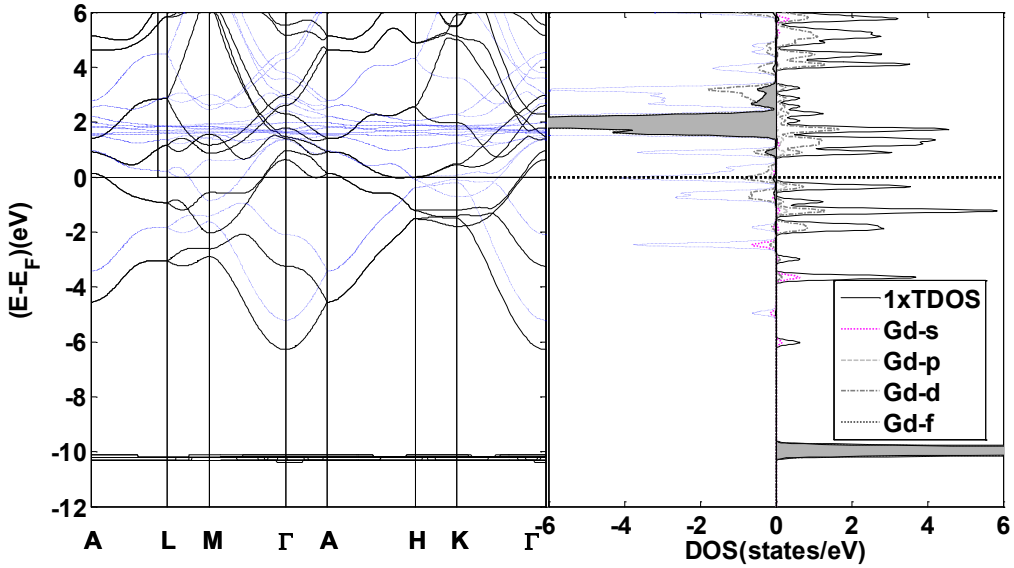

Fig. 5. *Band structure calculation and DOS within LDA+U calculation and 4f-band model*

Table 2. **Total energy (TE, in hatree) and energy differences, dE (in meV), between two phases FM and AFM**

	Approximation	TE, AFM phase	TE, FM phase	dE(meV) $=E_{FM}-E_{AFM}$
Calculation 1	LDA	-22545.5176615281	-22545.5173656716	8.1
	LDA+U	-22545.3641565677	-22545.3677646254	-98.2
Calculation 2	LDA	-22545.5176887987	-22545.5173456476	9.3
	LDA+U	-22545.3639499519	-22545.3678762767	-106.8

In order to do this, we carefully consider two sets of calculations. In *calculation 1*, lattice constants are taken from Shick et al. [13] and we let x-axis be along [110] direction. Numer of states are 90 of which the highest state is about 54 eV above E_F. In *calculation 2*, lattice constants are taken from Kurz et al. [11] and x-axis is along [010] direction. The number of states are 40 of which the highest state is about 19 eV above E_F. Basically, these two results of calculations should not be much different. For each calculation, we align magnetic moments to be parallel each other for FM and antiparallel for AFM and fix them during the self-consistent process to search for the minimum energy within both LDA and LDA+U calculations. The total energies are obtained by solving Eq. (1). We tabulate the results in Table II. Indeed, there are not much different between the two results of calculations. Accordingly, the calculated results show that in LDA calculation, the AFM is more stable with 8~9 meV lower than those of FM. Hower, in LDA+U calculation, the FM phase is more stable with 98~107meV lower than those of AFM. Our results are well agreement with results of Harmon el al. [20] in which LMTO+ASA calculation had been performed. And they found that within LDA calculation the energy difference is 8.2meV/atoms with AFM stable. In LDA+U calculation, the difference is -56.4meV/atom with FM stable. Shick et

al. [13] also found that FM is stable with energy different of about 63 meV (even this number is not clearly indicated for specific configurations in the paper) using LDA+U calculation within all-electron method. Kurz et al. [11] by using FLAPW-FLUER packages also demonstrated that the AFM phase is more stable over FM with -69meV in LDA calculation whereas the FM becomes more stable with energy difference of 34meV in the LDA+U calculation. By using the self-consistent semi-relativistic TB-LMTO-ASA method, Jenkins et al. [21] also argued that AFM is stable within LDA calculation with energy difference of 9.2 meV per atom. In another work, they used FP-LMTO method to prove both LDA and GGA giving AFM stable whereas in LMTO-ASA method, LDA gives AFM stable and GGA gives FM stable, with the energy difference of about 6mRy [22]. Petersen et al. [23] also used pseudo-potential method implemented by VASP package to testify that the orbital moment is very small and in GGA-PBE scheme, the energy different is ΔE=-7meV/atom with AFM stable whereas in GGA+U, calculated energy diference is 69 meV/atoms with FM stable. Our calculated results are excellent agreement with all these publications. And also 4f bands should be treated as valence bands with the Hubbard correction included, i.e. +U implementation [13].

3. CONCLUSION

FLAPW method is a very precise computational method to solve the modern material problems. It can well describe any system without shape approximation within atomic muffin-tin area, especially for dealing with the system with core structure, e.g. polarized wave functions. The use of input parameters should be very careful to obtain relevant results in the f compounds. The calculations applied for Gd show that Gd-4f can be treated either core, semi-core or valence states in some particular cases. The LDA scheme gives underestimated equilibrium lattice constants. Beyond this, it predicts excited f states to localize strongly near Fermi enery thereby the valence band close to Fermi level. Moreover, LDA calculation leads to AFM stable over FM phase whereas in LDA+U calculation, FM phase is more stable. This is reason giving rise to LDA+U implemented throughout the study and it should be invoked in studies of f-electron compounds. All the results from LDA and LDA+U calculations are well consistent with previous publications, especially for the proof of magnetic phase stability.

Acknowledgments

The author thanks Prof. Miyoung Kim at Sookmyung Women's University for the help and supervision.

REFERENCES

1. P. Hohenberg and W. Kohn (1964), Phys. Rev. 136, B864.
2. W. Kohn and L. J. Sham (1965), Phys. Rev. 140, A1134
3. E. Wimmer, H. Krakauer, M. Weinert, and A. J. Freeman (1981), Phys. Rev. B 24, 864
4. S. Youn and A. J. Freeman (2001), Phys. Rev. B 63, 085112.
5. M. Kim, A. J. Freeman, and C. B. Geller (2005), Phys. Rev. B 72, 035205.
6. T. Van Quang and K. Miyoung (2016), J. Korean Phys. Soc. 68, 393